CrossMark

ORIGINAL ARTICLE

Cytoarchitecture and neurocytology of rabbit cingulate cortex

Brent A. Vogt[1,2]

Abstract The rabbit cingulate cortex is highly differentiated in contrast to rodents and numerous recent advances suggest the rabbit area map needs revision. Immunohistochemistry was used to assess cytoarchitecture with neuron-specific nuclear binding protein (NeuN) and neurocytology with intermediate neurofilament proteins, parvalbumin and glutamic acid decarboxylase. Key findings include: (1) Anterior cingulate cortex (ACC) area 32 has dorsal and ventral divisions. (2) Area 33 is part of ACC. (3) Midcingulate cortex (MCC) has anterior and posterior divisions and this was verified with extensive quantitative analysis and a horizontal series of sections. (4) NeuN, also known as Fox-3, is not limited to somata and formed nodules, granular clusters and striations in the apical dendrites of pyramidal neurons. (5) Area 30 forms a complex of anterior and posterior parts with further medial and lateral divisions. (6) Area 29b has two divisions and occupies substantially more volume than in rat. (7) Area 29a begins with a subsplenial component and extends relatively further caudal than in rat. As similar areal designations are often used among species, direct comparisons were made of rabbit areas with those in rat and monkey. The dichotomy of MCC is of particular interest to studies of pain as anterior MCC is most frequently activated in human acute pain studies and the rabbit can be used to study this subregion. Finally, the area 30 complex is not primarily dysgranular as in rat and is more differentiated than in any other mammal including human. The large and highly differentiated rabbit cingulate cortex provides a unique model for assessing cingulate cortex, pain processing and RNA splicing functions.

Abbreviations
A30C	Area 30 complex
ACC	Anterior cingulate cortex
AD	Anterodorsal thalamic nucleus
aMCC	Anterior MCC
BSA	Bovine serum albumin
GAD	Glutamic acid decarboxylase
MCC	Midcingulate cortex
NeuN	Neuron-specific nuclear binding protein
NFP	Non-phosphorylated intermediate neurofilament H proteins
PBS	Phosphate-buffered saline
pMCC	Posterior MCC
PSF	Polypyrimidine tract binding protein associated splicing factor
PV	Parvalbumin
RSC	Retrosplenial cortex
RSG	Retrosplenial granular cortex

✉ Brent A. Vogt
bvogt@twcny.rr.com

1 Cingulum Neurosciences Institute, Manlius, NY, USA

2 Department of Anatomy and Neurobiology, Boston University School of Medicine, Boston, MA, USA

Introduction

Brodmann (1909) presented the first cytoarchitectural map of rabbit cingulate cortex and made a number of observations that need reconsideration in the context of the past decades of structural and functional studies. He observed

an anterior and posterior division of area 32 and no ecto-callosal area 33. While he observed anterior and posterior divisions of area 30 in the flying fox, he claimed it was not present in rabbits and termed the dorsal dysgranular field area 29d. Area 31 was located in and dorsal to the splenial sulcus with anterior and posterior divisions in the flying fox, but not in the rabbit. Ectosplenial area 26 was shown rostral to area 29a and area 29c extended quite far posterior. Of particular note was his placement of area 23 which he recognized was not granular, as it is in primates, but placed it there due to location. This is the posterior part of midcingulate cortex (MCC) as discussed in the present study.

The particular importance of MCC is apparent in studies of human nociception and movement. Acute noxious stimuli consistently activate the anterior portion of MCC (Vogt 2005; Farrell et al. 2005) which is involved in the anticipation and prediction of noxious stimuli (Porro et al. 2002, 2003) and has a skeletomotor output system in the cingulate sulcus that provides for avoidance (nocifensive) behaviors (Vogt and Sikes 2009). Validating its role in motor function, Talairach et al. (1973) showed that electrical stimulation of MCC evoked responses of the fingers, hands, lips and tongue to form simple movements such as touching, leaning, rubbing, stretching, sucking or licking. Cingulotomy ablations in this region have long been known to alter affective responses to noxious stimuli (Ballantine et al. 1967). As we have been unable to identify two parts of MCC in rodents (Vogt and Paxinos 2014), the presence of such divisions in rabbit cortex would provide an experimental animal for studies of pain processing and exploring this dichotomy is a primary goal of the present study.

Numerous recent advances in other species suggest that a major revision of our rabbit map (Vogt et al. 1986) is in order. (1) Area 32 has dorsal and ventral divisions in rodents (Vogt and Paxinos 2014) that were based on efferent connections (Gabbott et al. 2005) and they may be present in rabbit. (2) Although MCC has been observed in rabbit (Vogt 1993), it is not known whether it has two subdivisions as in monkey (Vogt et al. 2005) or only one as in rodents (Vogt and Paxinos 2014). (3) Retrosplenial areas 29 and 30 have anterior and posterior divisions in rodents (Vogt and Paxinos 2014) and human (Vogt et al. 2016) that may be present in the rabbit. (4) Preliminary observations of area 30 suggest a lateral division of area 30 that is not present in rodents. (5) Explore a few key comparative issues that guide the use of area designations in rabbit, rat and monkey. Immunohistochemistry was used to assess cytoarchitecture with neuron-specific nuclear binding protein (NeuN) and neurocytology with non-phosphorylated intermediate neurofilament protein (NFP) antibody SMI32, parvalbumin (PV) and glutamic acid decarboxylase (GAD). These target peptides were identified following a review of eight antibody reactions to determine which were most likely to demonstrate area differences throughout cingulate cortex. Those that were not pursued included calbindin, calretinin, met-enkephalin, and the mu-opioid receptor. These studies resulted in a major revision of the map of nine rabbit cingulate cortical areas to 20 areas, show that the area 30 complex is more differentiated than in any mammal thus far studied including the human and provide guidance for investigations of the molecular and functional organization of anterior MCC including studies of pain processing.

Materials and methods

Young adult rabbits (2.9 ± 0.47 kg) were used including one female, New Zealand Belted and four male/two female New Zealand White purchased from Harlan Laboratories (Cortland, NY). All animal procedures were approved by the Committee for the Humane Use of Animals at SUNY Upstate Medical University in Syracuse, New York. Rabbits were anesthetized with a lethal dose of sodium pentobarbital (50 mg/kg, i.p.), the heart injected with 1 ml 1 % sodium nitrite to dilate cerebral blood vessels and intracardially perfused with 300 ml cold (4 °C) saline (0.9 %; in 0.1 M phosphate buffer, pH 7.4), followed by 1 l of cold 4 % paraformaldehyde. The excised brains were placed in the refrigerator for 3 days of post-fixation, they were cryoprotected in sucrose (10, 20 and 30 % until they sank in each solution), frozen in a cryostat, and sectioned at 40-μm thickness into six coronal series and two horizontal series from female rabbits (2.8 kg each). Free-floating sections were pretreated with 75 % methanol/25 % peroxidase, followed by 3 min with formic acid (37 %), and then washed one time with distilled water and two washes in phosphate-buffered saline (PBS; pH 7.4; 5 min each). The primary antibody containing 0.3 % Triton-X-100 and 0.5 mg/ml bovine serum albumin (BSA) was incubated overnight at 4 °C. After incubation in the primary antibody, the sections were rinsed in PBS and incubated in biotinylated secondary antibody at 1:200 in PBS/Triton-X/BSA for 1 h in ABC solution (1:4; Vector Laboratories, Burlingame, CA) in PBS/Triton-X/BSA for 1 h followed by PBS rinses and incubation in 0.05 % 3,3′-diaminobenzidine and 0.01 % H_2O_2 in a 1:10 dilution of PBS for 5 min. After two 5-min rinses in PBS, sections were mounted. Table 1 provides information on the four antibodies used in this study. Antibody specificity was initially confirmed with blocking peptides or by excluding the primary antibody. Every case thereafter was assessed to determine the ideal dilutions generating the highest signal: noise reaction with trials from one of the six series. The

Table 1 Antibodies

Antibody	Type	Host	Immunogen	Concentration	Source/cat. no.	RRID
NeuN	Monoclonal	Mouse	Fox-3	1:1000	Chemicon/MAB377	AB_2298772
SMI32	Monoclonal	Mouse	Neurofilament H	1:10,000	Sternberger/SMI-32	AB_2315331
PV	Polyclonal	Goat	PV	1:3000	Chemicon/AB_15738	AB_838236
GAD	Monoclonal	Mouse	GAD65	1:5000	Chemicon/MA351R	AB_94905

only reaction for which a blocking peptide was not available was NeuN as it has only recently been identified to be Fox-3 (Kim et al. 2009) after the present tissue had been prepared. However, the specificity of staining for neurons was evaluated in many cases by counterstaining with thionin; only neurons were labeled and glia were not reactive with NeuN confirming the level of specificity required for these studies. Since SMI32 identifies a subset of neurons, some cases were counterstained with thionin to verify the layers in which labeled neurons and dendrites were located and associations of vertically oriented dendritic bundles to groups of neurons in superficial layers.

Sections were photographed at 10X–200X with an Optronics digital camera (Goleta, CA) mounted on a Nikon microscope (Eclipse 400). The black and white images were adjusted for brightness, contrast and evenness to balance sections within a figure and enhance architecture comparability at different anteroposterior levels of cingulate cortex. The only instance in which color balance was applied was for counterstained SMI32 sections in which the blue wavelength was reduced to enhance differentiation of the brown reaction product from the thionin-stained

chromatin. Higher contrast was applied to emphasize cellular boundaries and cytoarchitectural features as discussed below.

The flat map procedure involved selecting the case with the most robust immunoreactivity for the four selected markers (male 2.5 kg), NeuN sections were photographed at 40X, entered into Adobe Photoshop (CS6) and distances measured with the measurement tool at the cortical midpoint at the top of layer Va. The map has a resolution of 240 μm based on the distance between one and six sections. The cortex was flattened vertically from the corpus callosum and the values used to plot the extent of each area along each section as done previously (Vogt et al. 1995). The map based on coronal sections was slightly modified to account for observations made in the horizontal series; e.g., the dorsal aMCC and pMCC areas are somewhat broader in rostrocaudal extent than their ventral counterparts.

Our flat maps are an approximation of border locations to guide connection, receptor binding and other histological and neurophysiological studies. Of course, there are variances among animals and short transitions between cytoarchitectural areas. To avoid these problems, the

Fig. 1 Approach to quantifying neuron densities and somal sizes with NeuN. **A** The centroid of area p24a′ was selected, photographed at 200X and enlarged in Photoshop to 1200X for counting (**B**). **C** 400X photographs were taken of layers Va and Vb separately. **D** These were entered into Photoshop and enlarged to 1600X. **E** Exposure levels were adjusted such that overlaying neurons could be detected (*arrowheads*) and outlined and the area of each soma recorded
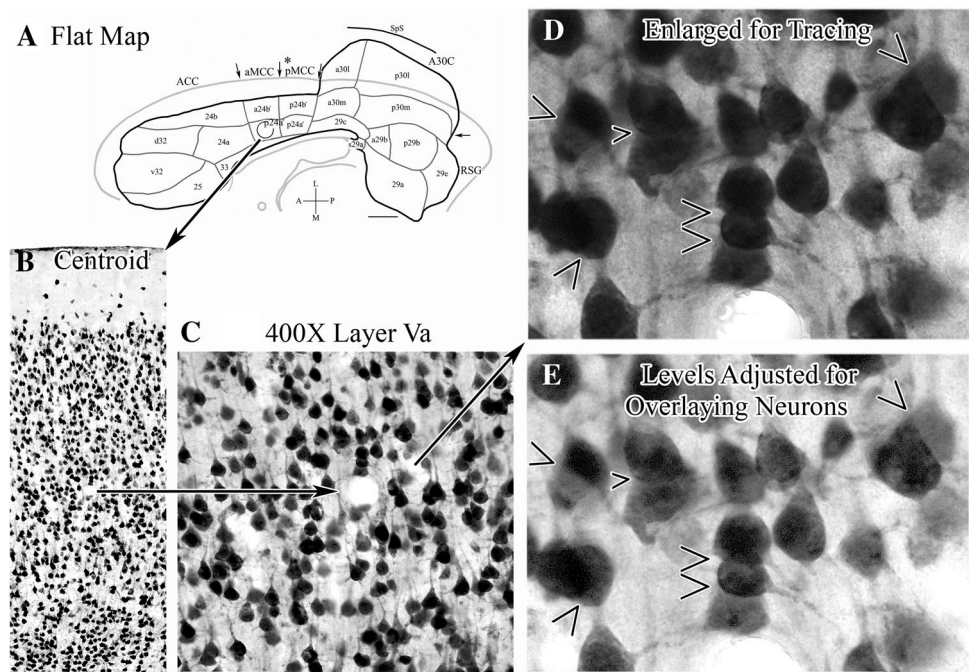
photographs for this study were generated in the centroid of each area as shown in Fig. 1. A centroid is the approximate middle of an area in the anterior–posterior, dorsal-ventral, and medial–lateral planes of section. Investigators interested in using the flat map are encouraged to identify the centroid(s) in their preparations with the flat map as a guide. Then, a reconstruction can be pursued for each case with the available staining. If NeuN sections are not available, Nissl-stained sections (cresyl violet, silver stain, thionin, neutral red) can be used to correlate with my images at the area, laminar or cellular levels of analysis.

Quantification for NeuN, SMI32, and PV involved the following steps as shown in Fig. 1.

1. NeuN, Black and white photographs were taken at 200X final magnification for a constant 750 μm width of cortex and imported into Photoshop, guidelines placed at the borders of each layer, enlarged to 800X and the levels adjusted to enhance differentiation of overlying neurons. Each neuron was counted, marked to avoid double counting, and the mean ± SD calculated for three sections in four cases. For calculation of neuron areas in layer V, 400X photographs were taken of layers Va and Vb separately, entered into Photoshop and guide lines placed at the top and bottom of each layer. The image was enlarged to 1200X (Fig. 1D) and the levels adjusted such that overlaying neurons could be identified (Fig. 1E) to enhance drawing cell boundaries for both neurons. Each neuron soma was outlined with the lasso tool and the area recorded. Neurons that were less than half within the region of interest were excluded and, when the boundary of the soma and apical dendrite was difficult to determine, the first node of NeuN was used to identify the apical dendrite (see "Results"). Each recorded neuron was marked to avoid double counting and the section resurveyed at 800X to assure none were missed. Three sections from three cases were used to determine large- (mean + 1 SD; >317 μm^2), medium- (mean ± 1 SD) and small- (mean − 1 SD; <157 μm^2)-sized neurons for a sample size of 4469 somata. Student t tests, one way, two sample of unequal variance were used to assess differences in neuron densities by layer.

2. SMI32. Black and white or color photographs were taken for SMI32-treated sections only or counterstained sections, respectively, of layer Va and Vb separately. The photographs were entered into Photoshop and guidelines set for equal areas in layer Va (total area assessed 781,220 μm^2) and Vb (total area 605,000 μm^2) so the total number of neurons was comparable for areas a24a′ and p24a′. The photographs were enlarged to 1200X and each SMI32+ soma with a negative-image nucleus and associated SMI32−

immunoreactive apical and basal dendrites was outlined to avoid counting fragments of neurons, the area of each soma recorded and the neuron marked to prevent double counting. Figure 6 shows examples of neurons that were so analyzed. The sections were resurveyed at 800X to assure that no somata had been overlooked. The mean ± SD was calculated for all neurons in layers Va and Vb for each of the two areas from three sections in three cases for a total of 887 somata with a mean area of 256 ± 113 μm^2. As large SMI32+ neurons are used to define area a24a′ qualitatively, large neurons were defined as the mean + 1 SD or >369 μm^2.

3. PV, Black and white photographs were taken at 100X and entered into Photoshop, adjusted for contrast, enlarged to 800X, and labeled neurons counted and marked for three sections each from three cases and reported as the mean ± SD.

Results

Flat map

Figure 2 presents the topography of areas in a flat map with the boundaries of each region/subregion shown and marked with arrows: ACC, aMCC, pMCC, retrosplenial area 30 complex (A30C) and retrosplenial granular (RSG) cortex. The medial surface outline is shown for orientation and does not match exactly the flat map because area dimensions were determined with measurements at the top of layer Va that are influenced by curvatures. Features not present in our previous map (Vogt et al. 1986) include: (1) dorsal and ventral divisions of area 32 (d32, v32) and a larger area 25, (2) area 33, (3) anterior and posterior midcingulate areas a24a′/b′ and p24a′/b′, (4) the complex of subareas of area 30 (a/p30l, a/p30m), (5) area 29c is reduced in extent, while area a30m is expanded, (6) subsplenial area 29a (s29a) and a much more extensive area 29a, (7) a two-part area 29b (a29b, p29b). The larger distribution of areas 25, 24b and 29a resulted from the measurement and reconstruction method instead of using the medial surface for reconstruction as done previously. The immunohistochemical preparations provided a much higher resolution of cytological architecture for most areas than is possible with Nissl-stained material because NeuN does not stain glia (Mullen et al. 1992).

Anterior cingulate cortex

An overview of anterior cingulate cytoarchitecture is provided in Fig. 3 with eight pairs of NeuN/SMI32

Fig. 2 *Flat* map of rabbit cingulate cortex plotted onto a medial surface for reference with each region and subregion borders marked (*arrows*). Level of Bregma noted with an *asterisk*. This *map* details the topographical distribution of each area identified immunohistochemically. *Scale bar* 2 mm
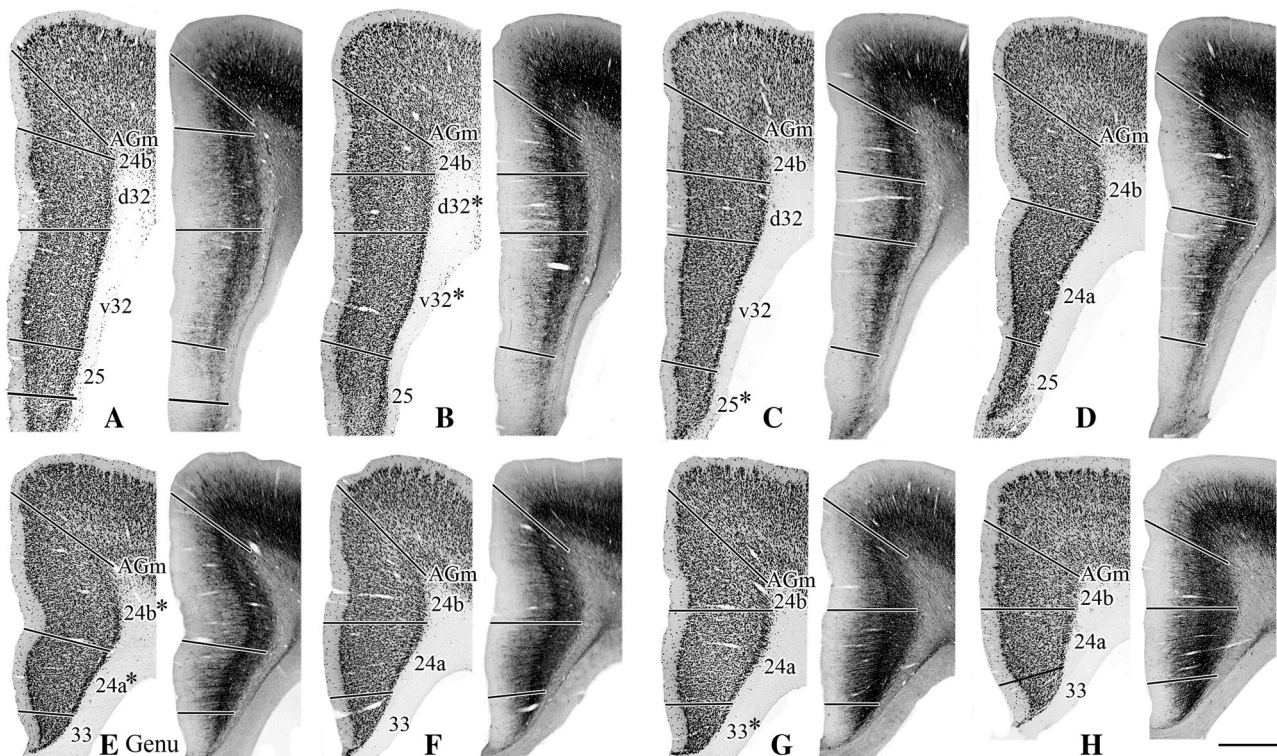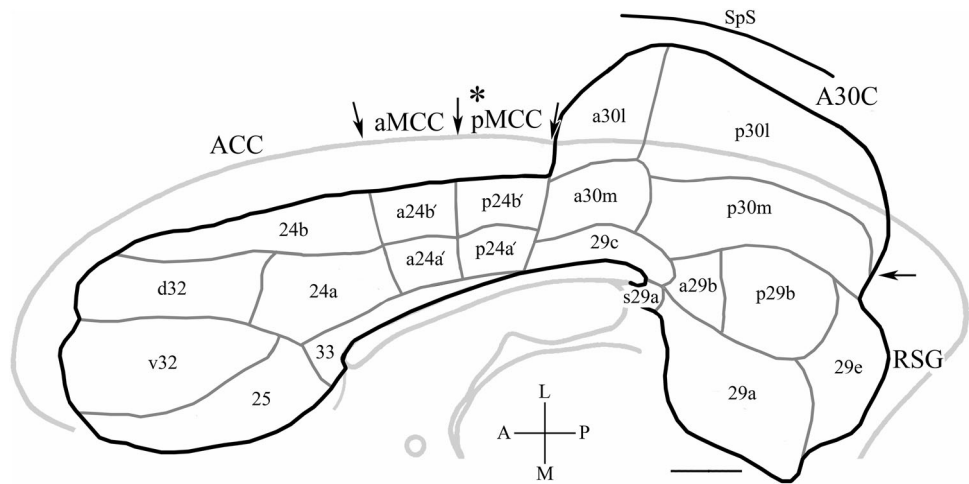

Fig. 3 Macrophotographs of pairs of NeuN and SMI32 immunoreacted anterior cingulate areas. **E** Is at the level of the genu of the corpus callosum. *Asterisks* next to some areas indicate the levels at which sections were selected for Fig. 4. The overall relative differences among ACC areas are employed to further assess the microstructure of each area. *AGm* medial agranular motor cortex (also M2). *Scale bar* 1 mm

immunoreacted sections. Area 24b extends along almost the full rostrocaudal extent of ACC. It has many large pyramids in layer Va where there is also a dense network of NFP+ dendrites. There is a consistent NFP-expressing population of neurons in layer IIIc, though not as dense as in layer Va, and a moderately dense plexus in layer VI and bottom of layer Vb. Area 32 has fewer NFP-expressing neurons in layer IIIc and the plexus in layer VI condenses into a thinner and moderately dense layer. Figure 3B shows five densities of SMI32-immunoreactions starting with greatest in the medial motor area AGm (M2) with sequentially less in each ventral area until there is almost none in area 25. Area 24a, particularly at caudal levels (Fig. 3G), has more NFP in all layers than area 24b, although they do not appear to be particularly prominent in layer VI. Finally, the differentiation of area 32 into dorsal

Fig. 4 Triads of microphotographs (NeuN, SMI32, PV) of ACC areas. The *lines* in **A** and **B** denote the borders between areas d32/v32 and 24b/24a, respectively, with *asterisks* showing the borders between layers that are identified at the top of each series. *Scale bar* 500 μm
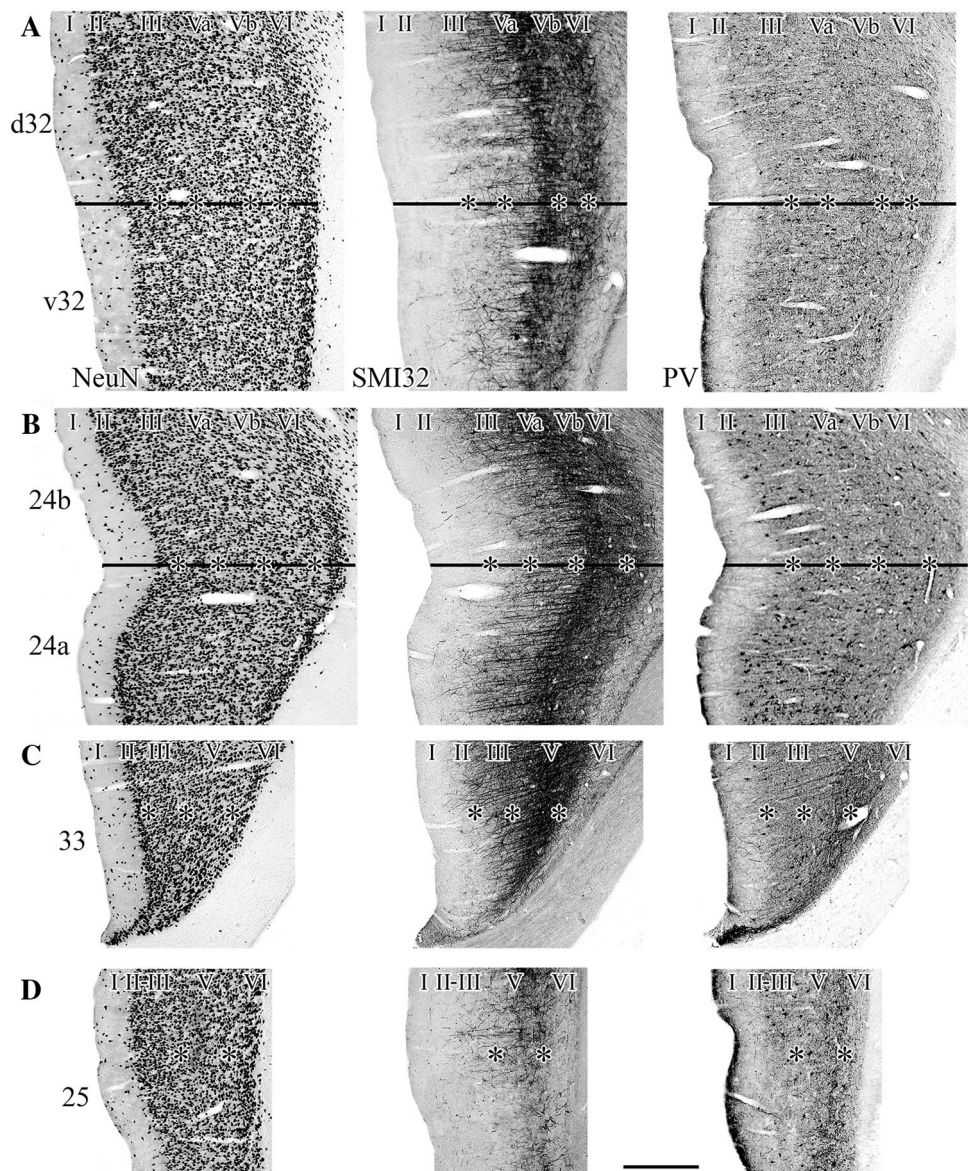
and ventral divisions was originally based on the ACC projection studies of Gabbott et al. (2005) in the rat that was found to have a cytoarchitectural substrate (Vogt and Paxinos 2014). This differentiation is prominent in rabbit and the details of neurocytology are better appreciated at higher magnifications as in Fig. 4.

The asterisks next to area designations in Fig. 3 denote levels at which microphotographs were taken for Fig. 4. Dorsal area 32 in comparison to the ventral division (Fig. 4A, line separates their border) has a more dense layers II and III with larger pyramids and those in layers Va and Vb are also larger and express substantially more NFP (Fig. 4A, SMI32). Layers III and VI of area v32 also have a much reduced NFP+ dendrites and somata. In terms of PV, layer Va has noticeably more PV+ somata in area d32 than v32, but all other layers appear to be similar. Area 24b vs area 24a has larger and more dense pyramids in layers III, V and VI (Fig. 4B, NeuN), robust SMI32 reactivity is in layers V and VI and there is a moderately dense plexus in layer III. Although there may be a few more PV+ neurons in layer III of area 24b, there are no further differences with area 24a. Finally, area 33 has poorly defined layers II–III, no subdivisions of layer V and there is a very thin layer VI. The NFP expression, however, is substantial in layer V particularly in comparison to area 25 which has virtually no NFP expression. Area 25 has the least laminar differentiation of the ACC areas with low densities of PV+ neurons in layer II–III and more in layer V that are reduced in number in ventral parts of area 25 where they mainly reside in layer V.
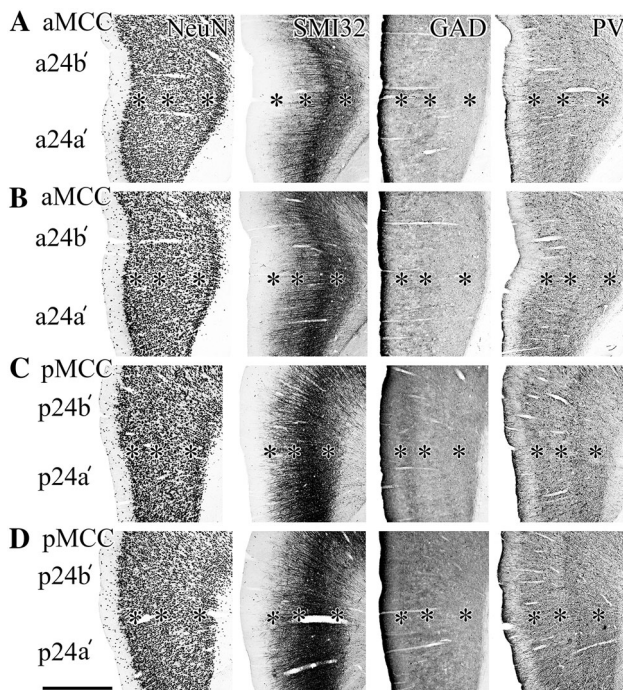
Fig. 5 Macrophotographs through four levels of MCC. The *asterisks* mark the borders between layers II/III, III/Va and Vb/VI. The rabbit MCC dichotomy is critical as rodents do not have this organization. *Scale bar* 1 mm
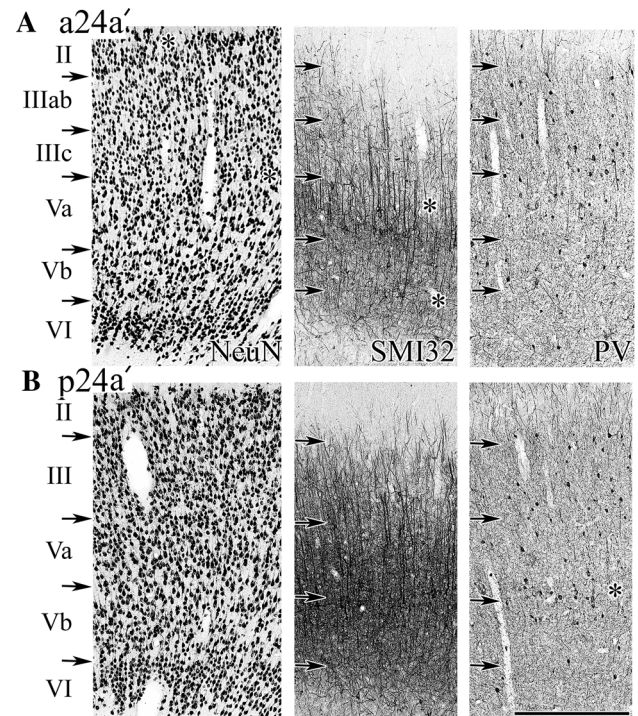

Fig. 6 The MCC dichotomy shown with NeuN, SMI32 and PV. The asterisks in a24a′ (SMI32) emphasize the layer Va and Vb pyramids; the former of which shows where the higher magnification photograph was taken (SMI). In a24a′-PV the asterisk notes the high density of PV+ somata in layer IIIc. In contrast, p24a′ has a higher density plexus in layer Vb. The profound differences between the two parts of MCC are emphasized at higher magnification (SMI) where the large NFP-expressing neurons in layer Va are shown in Fig. 8 and compared to p24a′ where there are substantially fewer such neurons. Thus, the anterior and posterior parts of rabbit MCC are substantially different. *Scale bar* 500 μm

Midcingulate cortex

The MCC has only one division in the mouse and rat based on Nissl staining (Vogt and Paxinos 2014) and a major issue is whether or not this is true for the rabbit. Since area 24′ is agranular, sections were surveyed from the splenium beginning at the first instance where layer IV was not present rostral to area 29. As a key feature of area 24′ is large layer V pyramids, the survey continued until these were greatly reduced heralding the beginning of ACC. Four pairs of sections are shown in Fig. 5 of the two divisions of area 24′ in aMCC and pMCC. In contrast to area p24b′, a24b′ has particularly pronounced layers Va and VI (NeuN), NFP extends throughout layer VI (SMI32) and they are more dense in layer Va. PV is more intense in layers V and VI of pMCC; a difference that trended to significance in the analysis below and is supported by GAD immunoreactivity. Area p24′ has substantially higher GAD levels in layers I–III than does area a24′.

Figure 6 demonstrates the details of aMCC and pMCC architecture in NeuN and SMI32 preparations of areas a24a' and p24a'. Features of area a24a′ vs p24a′ include (a) larger neurons in layers II and VI (NeuN), (b) prominent large pyramids in layer Va (NeuN; SMI32), (c) layer III is differentiated into two parts (IIIab and IIIc; NeuN), although there are some large neurons in the top of layer III in area p24a′ (NeuN), (d) the number of PV+ neurons in

layer IIIc is higher, while the number in the deep part of layer Va of p24a′ (asterisk) is higher.

The borders of the midcingulate areas were assessed in a horizontal series shown for four pairs of matched sections in Fig. 7. The single asterisk is dorsal to the splenium, while the double asterisk is on the genu of the corpus callosum. Overall, the borders are relatively sharp between adjacent areas and they are confirmed with the paired NeuN and SMI32 sections. Of particular note is the wider rostrocaudal extent of areas a24b′/p24b′ (A) in comparison to areas a24a′/p24a′ (B). In both pairs of areas the large layer V neurons (parentheses) are apparent even at this low magnification with those in areas a24a′ and a24b′ being larger and less densely packed. To clarify the border between areas p24b′ and a30m in the top pair of sections, their border was magnified for Fig. 8A (NeuN) and B (SMI32). While all other photographs were taken in the centroid of each area, these two are from their border (marked with lines). The beginning of a layer IV appears in area a30m, layer V neurons are somewhat smaller, and
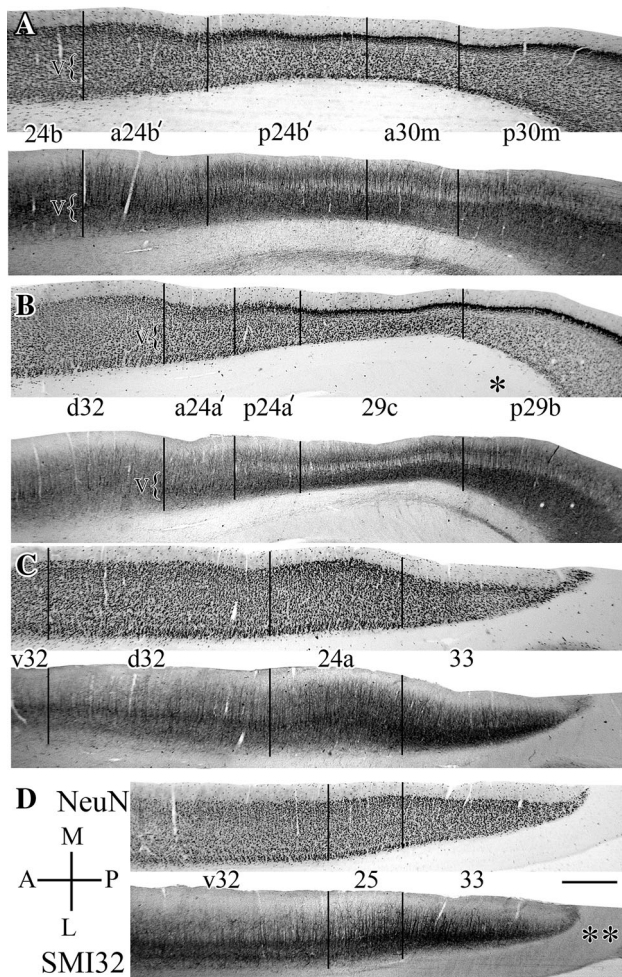
Fig. 7 Pairs of NeuN and SMI32 sections taken horizontally from four levels starting in **A** dorsal to the corpus callosum, **B** close to the splenium (*asterisk* marks the approximate level of the splenium just ventral to the section), **C** rostral to the corpus callosum and **D** is close to the ventral edge of the genu (*double asterisk*). *Borders* between areas are relatively sharp and the two preparations confirm each other. *Scale bar* 1 mm

layer VI is less dense than in area p24b′. The SMI32 preparation shows a higher density of neurons and dendrites in layer II and top of layer III as well as more clumps of very large neurons and their associated apical dendrites in layer V.

Areas rostral to the genu (Fig. 7C, D) appear as predicted from coronal sections and the architecture in both preparations is also as noted above from coronal sections. In a second horizontal case, a pair of electrodes was placed in area a24b′ as shown in Fig. 8C–E. These electrodes were 1.5 mm from Bregma to verify the position of the area border in the flat map in Fig. 2. A third electrode penetrated area d32 (slightly different positions were due to the angle of the electrode). The area borders were closely matched in thionin (D) and SMI32-immunoreacted
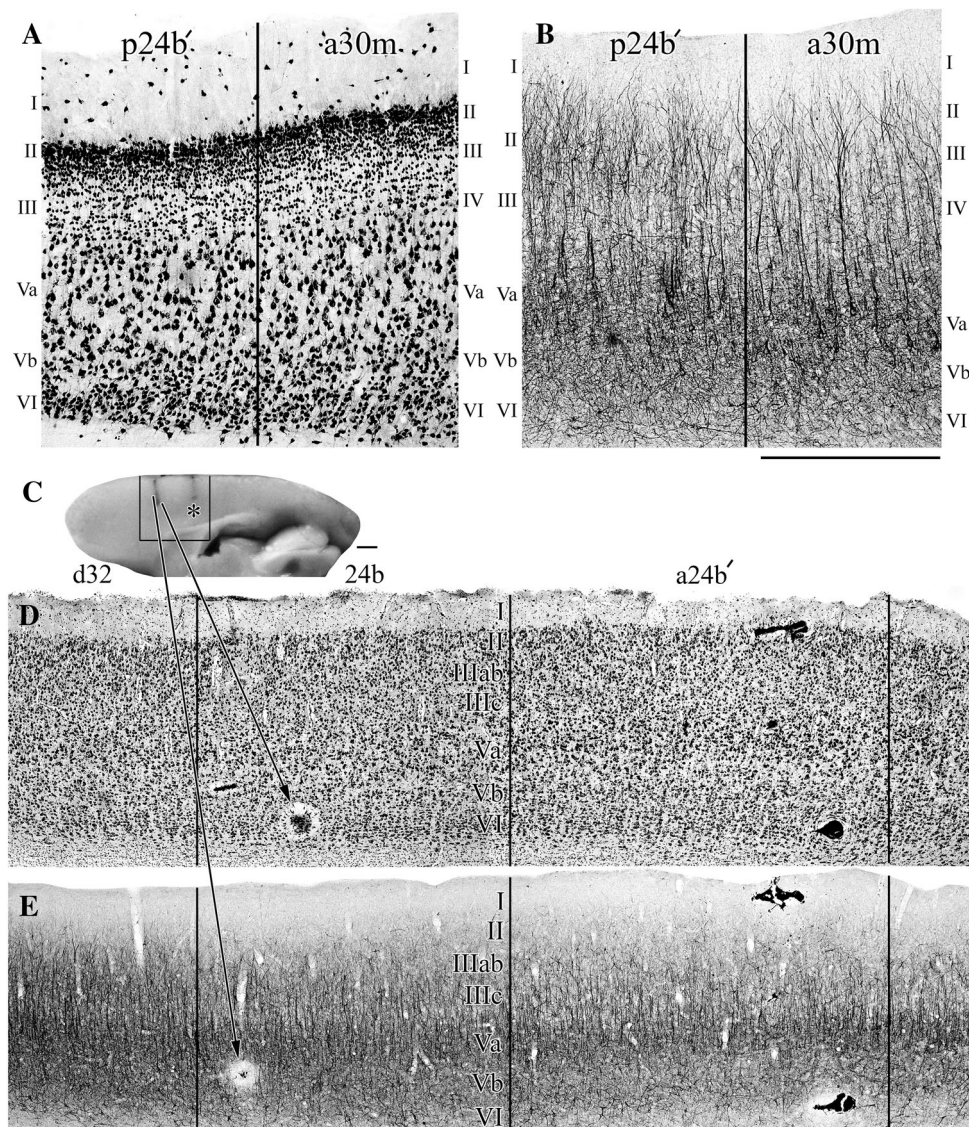
(E) sections. In this plane of section, area 24b can be seen to have a greater density of neurons in layer VI than in area a24b′ and the latter area has more large neurons in layers Va and Vb. Also of note is the heavier SMI32-immunoreactivity throughout layer III of area d32; the progression from low to high levels is seen between areas a24b′, 24b and d32.

Subcellular localization of NeuN/Fox-3

Since the NeuN antibody is the key marker used for distinguishing cytoarchitecture and quantitative analysis at high magnification below, it was observed that dendritic labeling was not uniform. The NeuN antibody applied to rabbit identifies Fox-3 not only in nuclei and perikarya as in rat (Kim et al. 2009) but also in the rabbit there are dendritic nodules, granules and striations of reaction product as well as plasmalemmal associations that suggest a complex pattern of RNA editing by Fox-3. Figure 9 shows examples of these localizations in MCC, but they can also be observed throughout other cingulate areas. The locations of RNA nodules are marked along the apical dendrites of three thionin-stained pyramids (Fig. 9A–C). Thionin staining is too faint, however, to detect nodules beyond ~45 μm from the soma and the many other localizations, particularly in large pyramids reacted with NeuN, is quite robust. The nodules of aggregated Fox-3 are observed in the apical dendrites of most pyramids and in the largest pyramids they are up to 70 μm from the soma (Fig. 9F–K). The apical dendrites of two pyramids (E, I) were enlarged by 150 % to enhance visualization of the nodules. The largest ones are near the soma, while they are smaller as a function of the distance from the soma. Rarely, there are large basal dendrites that express granular deposits that do not form nodules (Fig. 9D). Inverted pyramids in layer Vb also usually express nodules in their apical dendrites (Fig. 9M) and medium-sized, multipolar neurons occasionally express them (Fig. 9E).

Figure 9G–I has arrowheads marked with asterisks to denote granular deposits and there are striations between granular deposits (Fig. 9H, I) where they are marked with arrows. There are also striations between nodules (Fig. 9K) where they are between the 2nd and 3rd and 3rd and 4th nodules counting from the soma. In rare instances when the pyramid is cut in the best plane of section and the nuclear reaction does not interfere with detection, reaction product lines the plasmalemma (Fig. 9L). Finally, a survey of layers II–III and VI showed similar distributions of NeuN in areas a24a′ and p24a′. While the large, layer V pyramids have the most pronounced localizations noted here, they are not unique to this layer. Thus, rabbit cingulate pyramids have a wide range of Fox-3/NeuN morphologies that are observed in most pyramids. RNA editing by Fox-3 and

Fig. 8 A NeuN and **B** SMI32 are from the border of areas p24b′ and a30m at levels approximating those of the first two sections in Fig. 7 (*lines* demarcate their border). While area differences are less pronounced at borders in comparison to those taken at centroids, differences between both areas are evident as detailed in the text. In a second horizontal case, a block of cingulate cortex (*box* in **C**) was cut and stained for thionin (**D**) and SMI32 (**E**). Two electrodes were in area a24b′, 1.5 mm rostral to Bregma. The borders between adjacent areas are relatively sharp in both preparations. *Scale bars* from top to bottom; 1, 2 and 1 mm

NeuN+ neuron densities and sizes

Quantification was undertaken to calibrate qualitative size differences among neurons (small, medium, large) and to test the hypothesis that the two MCC divisions are statistically different from one another. Table 2 shows the mean ± SD of the number of NeuN+ neurons in each layer of both MCC areas. While layer III in area p24a′ is thicker than in area a24p′ (450 vs 310 μm) and layer Vb of area p24a′ is thicker than in area a24a′ (300 vs 240 μm), other layers are of similar thickness. There were no differences in neuron numbers in any layer. The similarity in neuron numbers for each area belies the MCC phenotype and, since neuron numbers are not a criterion for their differentiation, the somal area of each neuron in layers Va and Vb was calculated to determine if neuron sizes differentiate them as suggested from qualitative observations. A total of 4469 neurons were analyzed and they had an average somal area of 237 ± 80 μm². Large neurons were defined as those with an area 1 SD over the mean for all neurons and, as predicted, area a24a′ had 33 % more large neurons in layer Va than area p24a′ and there were almost 50 % fewer large neurons in layer Vb of area a24a′ than in area p24a′. Small neurons were defined as the mean area for all neurons minus one SD and there were many small neurons in both divisions of area a24a′ layer V with 30 % more in layer Vb. Finally, medium-sized neurons are those with somal areas of 157–316 μm².
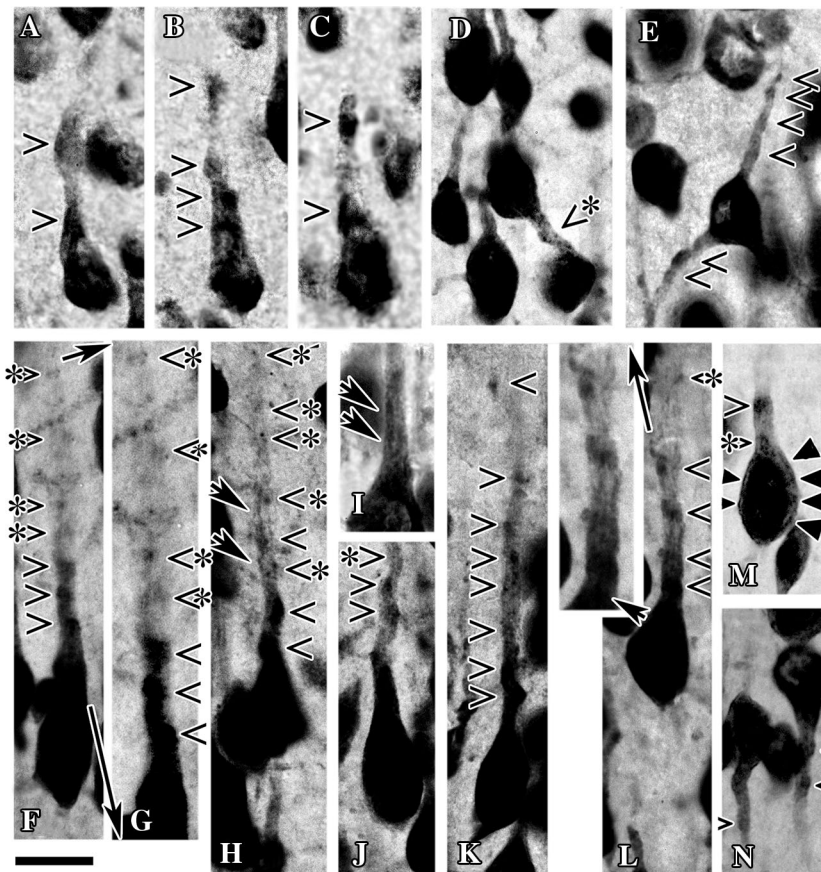
associated peptides likely contributes to protein synthesis throughout the apical dendritic tree as considered further in the "Discussion".

Fig. 9 NeuN/Fox-3 is localized beyond the soma in layer V of areas a24a′ and p24a′. **A–C** Large, thionin-stained pyramids with nodules of chromatin in their apical dendrites (*arrowheads*). All subsequent plates are of NeuN preparations. **D** A large basal dendrite with granular deposits (*arrowhead with asterisk*; also used for subsequent plates). **E** A medium-sized multipolar neuron with nodules. **F** Large pyramid with three nodules and four granular deposits in the apical dendrite. **G** A 150 % enlargement of (**E**). **H** Large pyramid with apical nodules and granular deposits as well as striations between the latter marked with two *arrows* **I**. Thicker striations in apical the dendrite. **J**, **K** Two examples of medium-sized pyramids with nodules and granular deposits. **K** Apical nodules in a pyramid with a 150 % enlargement to show the details of nodules which have striations of NeuN between the 2nd and 3rd and 3rd and 4th nodules counting from the soma. **M** Plasmalemmal-associated NeuN deposits in the perikaryon (*solid arrowheads*). **N** Two inverted pyramids in layer Vb with nodules. **A**, **K** Are from area a24a′ and **L**, **M** from p24a′. *Scale bar* 20 μm

SMI32+ neuron densities and sizes

A key feature of area a24a′ distinguishing it from area p24a′ is the large, SMI32+ neurons in layer Va (Fig. 6; SMI32) and Fig. 10 provides a higher magnification of this (compare A and B). In this latter figure (C, D, E, F), one can observe that apical and basal dendrites are emitted from the somata, not all SMI32+ neurons are the same size and the intensity of staining is not the same for all neurons. The total number of SMI32+ neurons in each part of layer Va did not differ between the two MCC divisions (Table 2), while there were 40 % more neurons in layer Vb of area p24a′ as also shown for NeuN above. The number of SMI32+ neurons in layer V, however, is not the distinguishing feature of area a24a′; it is the size of such neurons that differentiates these areas. The somal area of all SMI32+ neurons was calculated for 887 neurons with an average 256 ± 113 μm^2 somal area. Large neurons were defined as having an area one SD greater than the mean (317 μm^2) and there were almost 50 % more large, SMI32+ neurons in layer Va of area a24a′ than in p24a′, while there were no differences in layer Vb. Thus, the qualitative observations of large neurons differentiating the two divisions of MCC in layer Va with NeuN and SMI32 were confirmed with quantitative analysis.

PV+ neuron densities

A higher density of PV+ neurons in layer Va of area p24a′ is apparent in Fig. 6B. PV and there was a trend for more such neurons in area p24a′ of this layer (Table 2; a24a′ 15 ± 0.6 vs p24a′ 25 ± 9.9; t test, $p = 0.09$). The density of PV+ neurons in all other layers, however, did not differ for these two areas.

Table 2 Neuron numbers and sizes in MCC

	a24a′	p24a′
NeuN		
Layer		
I[a]	33 ± 5	30 ± 6
II[a]	314 ± 95	301 ± 28
III[a]	542 ± 36	512 ± 60
Va[a]	308 ± 50	296 ± 65
Vb[a]	282 ± 41	274 ± 43
VI[a]	334 ± 19	337 ± 32
V		
#Neurons	4469	
Mean area ± SD	237 ± 80 μm²	
Va[b]	**183 (+33 %**)**	138
Vb[b]	110	**164 (+49 %)**
Va[c]	136	121
Vb[c]	**162 (+30 %)**	125
SMI32		
Va		
#Neurons	254	247
Mean area ± SD	290 ± 118	275 ± 111
Vb		
#Neurons	161	**225 (+40 %)**
Mean area ± SD	211 ± 109	228 ± 96
V		
#Neurons	887	
Mean area ± SD	256 ± 113 μm²	
Va[d]	**52 (+49 %**)**	35
Vb[d]	12	18
PV ($p = 0.09$)		
II	6 ± 4.2	7 ± 0.6
III	21 ± 4	26 ± 7.2
Va	15 ± 0.6	25 ± 9.9
Vb	14 ± 5.1	16 ± 10
VI	8 ± 3.9	8 ± 4.2

Bold values indicate high percentage differences in neuron numbers

** Percent calculations where differences ≥30 %; large neurons used to differentiate these two areas in NeuN and SMI32 preparations. Difference in layer Va shows a trend based on t testing

[a] Mean # neurons ± SD

[b] Mean area +1 SD >317 μm² = large neurons

[c] Mean area—1 SD <157 μm² = small neurons

[d] Mean area + 1 SD >369 μm² = large neurons

As PV is expressed in GABAergic neurons, higher magnification, color photographs were taken of both parts of MCC to evaluate the possible higher level of GABA function in p24a′. Figure 11A, B shows this differentiation and emphasizes differences throughout the cortex and the a–c divisions of layer I. In combination with PV immunoreactivity there is a suggestion of greater GABA

control in pMCC; however, further quantitative studies of other calcium-binding proteins are needed to confirm this trend.

Retrosplenial cortex

The rabbit RSC has two significant variations compared to the rat and each retrosplenial division is shown with macrophotographs in Fig. 12 of NeuN and SMI32 reacted sections and in the comparative Fig. 18. First, granular area 29c is not as relatively extensive as in rat, area 29b has anterior and posterior divisions, area 29a begins just ventral to the splenium as in rat, but there is a subsplenial component (s29a), area 29a extends further caudally than in rat and area 29e emerges at the caudal end of areas 29a and p29b and is not present in rat. Second, while the rat area 30 has anterior and posterior divisions as does the rabbit, area 30 has additional variations including a lateral extension (areas a30l and p30l). Since most area 30 divisions have a robust layer IV and are not dysgranular as in rat, this subregion in rabbit is referred to as the area 30 complex (A30C).

Granular retrosplenial areas

Figure 13 shows area s29a in three preparations. Area s29a has a very thin layer IV compared to area 29a and uniform layers V and VI. There are few NFP-expressing neurons in layer V, although PV has a similar pattern to area 29a with a dendritic plexus in layer Ia and a dense plexus with somal labeling in layer II–III.

The asterisks next to area designations in Fig. 12 are the positions at which higher magnification photographs were taken for Figs. 13–15. Area 29a (Fig. 14) is poorly differentiated; i.e., it has few uniquely identifiable layers like area s29a. A dense layer II–III is noted in Fig. 14 (NeuN) that contains some NFP+ pyramids (SMI32) while layer V has a homogenous plexus of NFP+ dendritic processes some of which penetrate layer IV. Layer IV is broad and comprised small neurons, while layer V contains moderately sized pyramids. Although all granular retrosplenial areas have heavy GAD axonal labeling in the outer one-third of layer I (Fig. 14; GAD; layer Ia), area 29a has heavy GAD labeling throughout layer I and a pronounced plexus in layer IV. Finally, PV+ dendritic plexuses extend throughout layers I and II–III and moderate somal labeling in layer II–III and deep layer V and VI. Area 29e is caudal to area 29a and its expression of GAD and PV is similar to that of area 29a. The area 29e NeuN preparation, however, demonstrates a number of distinctions. Layers II and III are separated and layer III is wider than in other RSG areas. Although pyramids in layer Va are somewhat larger than in layer Vb, the latter neurons express substantially more NFP
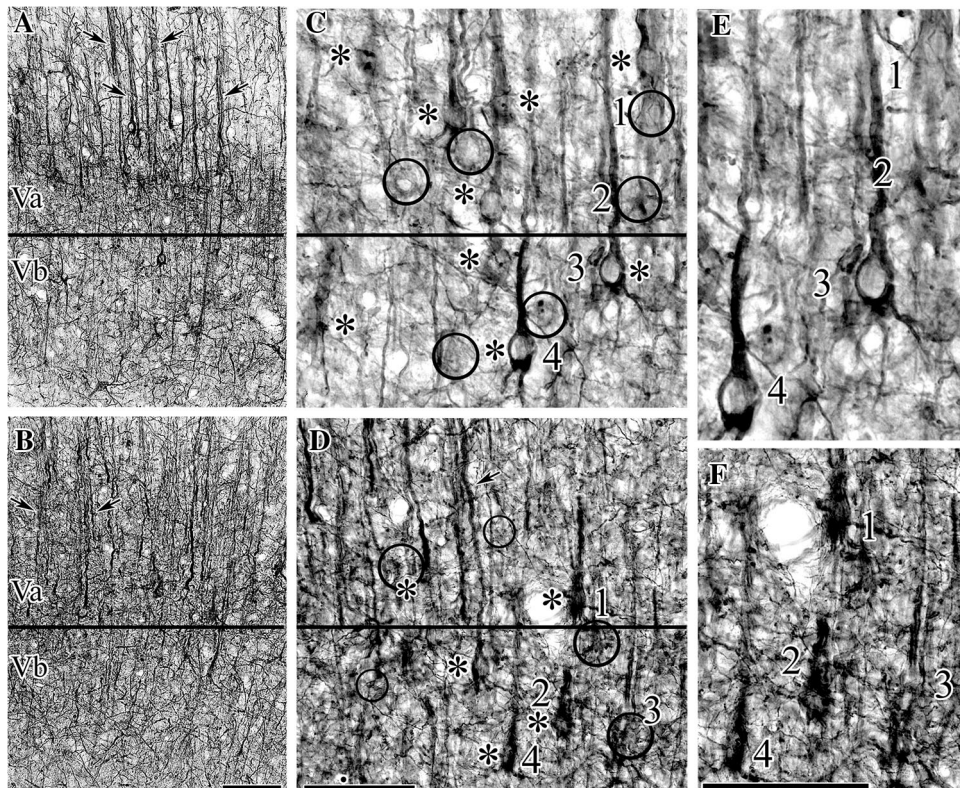
Fig. 10 Details of SMI32 labeling in areas a24a′ (**A**, **C**, **E**) and p24a′ (**B**, **D**, **F**) used for quantification. Differences in the density of large, immunoreactive pyramids in layer Va of both areas are obvious (**A** vs **B**). Some of the larger, apical dendritic bundles are noted with *arrows* throughout these plates. **C**, **D** Higher magnification of the border between layers Va and Vb. **C** *Asterisks* denote neurons that are heavily SMI32-immunoreactive and those with light reactions are *circled*. **D** *Asterisks* show the same heavily labeled neurons and the *circle* with an *asterisk* is a lightly labeled, small neuron. **E** Numbering

matched for the same neurons in **C**; lightly labeled neuron (*1*), heavily labeled, small neuron (*2*), and heavily labeled, large neurons from which apical dendrites are emitted (*3*, *4*). **F** Numbering matched for the same neurons in **D**; three neurons with heavy labeling of somata and apical and basal dendrites (*1*, *2*, *4*) and a small pyramid with a lightly labeled soma and moderately labeled apical dendrite (*3*). All of these neurons were assessed for somal areas in the quantitative analysis. *Scale bar* 100 μm

Fig. 11 A, **B** Higher magnification of GAD reactions in areas a24a′ and p24a', respectively. The GAD+ axons are more dense in all layers of area p24a′ than in a24a′. **C** Thionin-counterstained, SMI32 of area a30l shows clusters of dendrites formed by layer V pyramids that extend through layer III and pass by islands of neurons in layer II. The islands are marked with *arrowheads* and in two instances (*asterisks*) they appear to form chalices around the islands. *Scale bar* for **A**, **B** 1 mm, **C** 100 μm
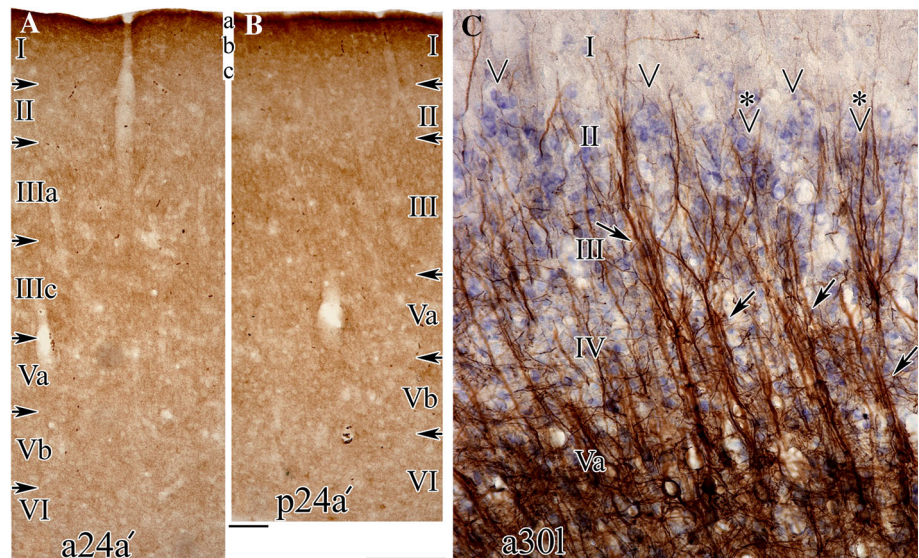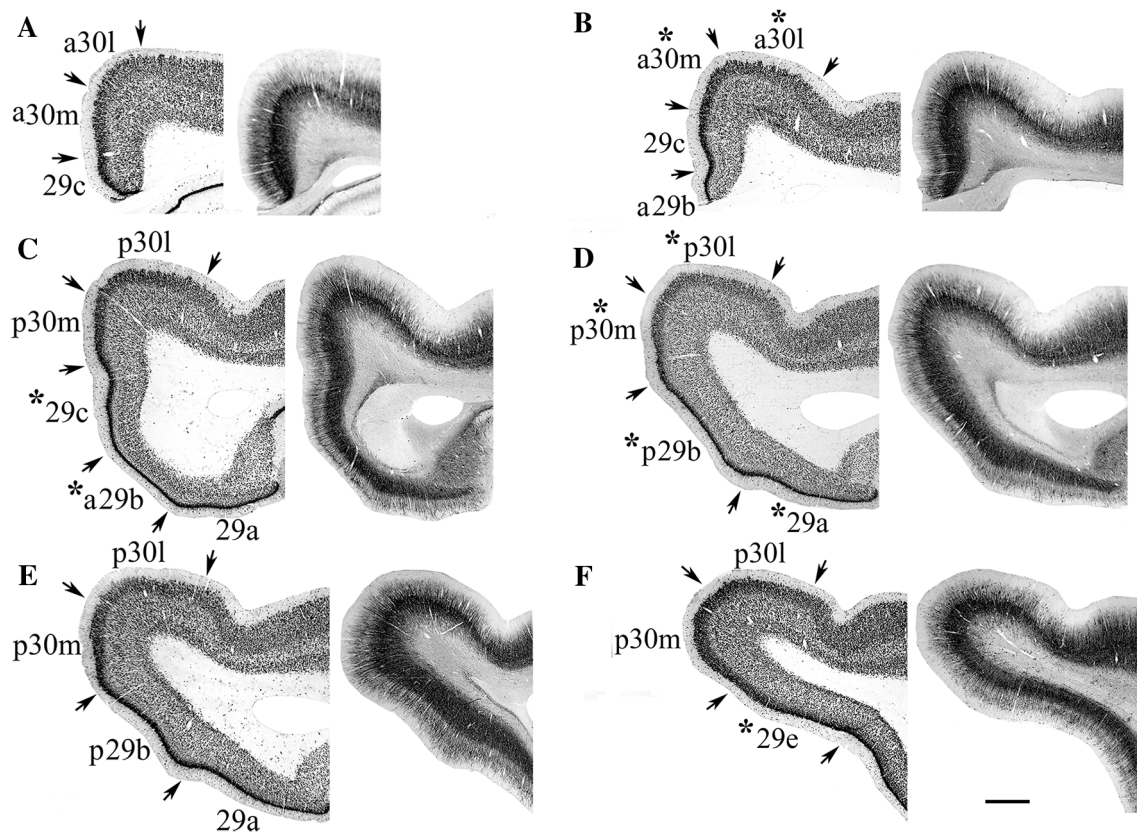
Fig. 12 Macrophotographs of six pairs of NeuN and SMI32 immunoreacted sections through RSC with each area delineated. The *asterisks* adjacent to some areas indicate the areas and sections that were magnified further for Figs. 14 and 15 providing a basis for detailed microanatomical studies. *Scale bar* 1 mm

(SMI32) and the NFP reaction is lower deep in layers Vb and VI.

All layers in area p29b are well differentiated (Fig. 14; NeuN) with layer Va comprised of medium-sized pyramids, layer Vb has larger pyramids that are not as densely packed as in Va, and a prominent layer VI; the latter of which is more pronounced than in other retrosplenial areas (NeuN). Layer II contains many NFP-expressing multiform neurons (SMI32), layer Va has the most dense dendritic plexus and many of the layer Vb pyramids are SMI32+. The GAD reaction is most dense in layers Ia and Ib, lighter in layer II–III and a moderate plexus is in layer IV. Finally, heaviest labeling of PV-expressing neurons and dendrites is in layer IV, there is a dense dendritic plexus in layer Ia, and a large number of somata are labeled in layer Va.

Area a29b has a substantially smaller volume than area p29b; comparing thicknesses in Fig. 14 and topography in Fig. 2. Layers II and III merge and layer V is generally homogeneous with a barely detectable layer VI. The NFP and GAD patterns are essentially the same as for area p29b. Parvalbumin expression is also similar for both areas, although fewer labeled somata are in layer V of area a29b.

Area 29c cytoarchitecture in rabbit is quite similar to that in rat (Fig. 14; NeuN) with a broad layer II–III, thick and well-defined layer IV, a two-part layer V and a layer VI of moderate size. The NFP pattern of labeling in particular distinguished this area from adjacent area a29b where there are many medium-sized pyramids in layer II–III and many more labeled somata throughout layer V. GAD labeling is high in layer Ia and there is a moderate density plexus in layer II–III. Parvalbumin-labeled somata are mainly in layers II–III and Vb.

Area 30 complex

Area 30 in the rat is dysgranular as it has a very thin layer IV (Vogt and Paxinos 2014). In the rabbit, however, only area a30m has a truly dysgranular layer IV, while the other divisions have a prominent layer IV (Fig. 15; NeuN). Area a30m also has a more dense layer II–III and relatively thin layers V and VI. Interestingly, NFP expression in layers II–IV of this area is the highest of any retrosplenial area both in terms of labeled somata and dendritic plexuses. Thus, most of the area 30 complex is not dysgranular in the rabbit and this term is not generally useful for rabbits.
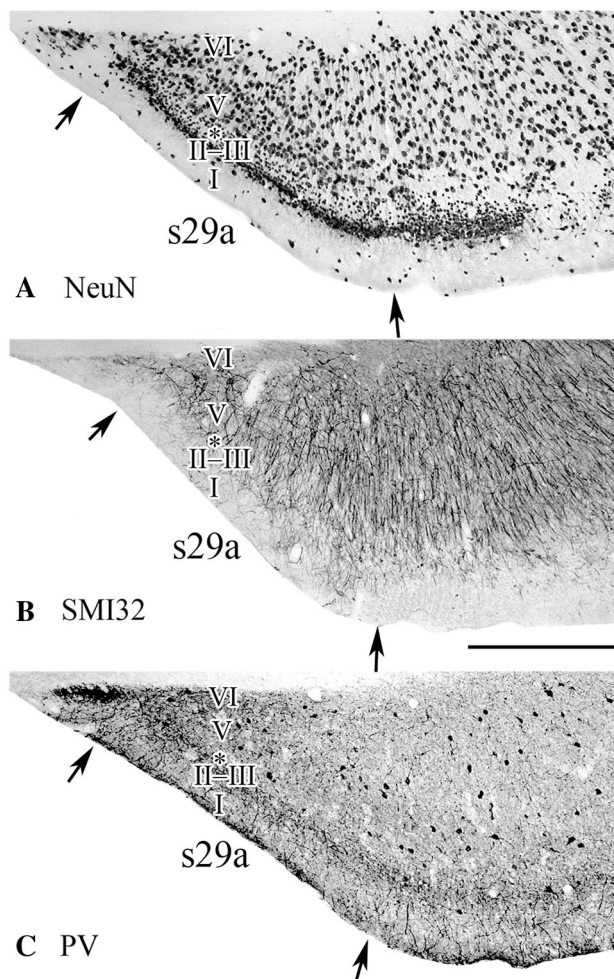
Fig. 13 Area s29a below the splenium of the corpus callosum (*upper left* of each image). The *asterisk* in each plate notes the extremely thin layer IV. Dorsal to this area is the indusium griseum and ventral there may be the beginning of area 29b. This area is of interest because it is not present in primates. *Scale bar* 500 μm

Area a30l differentiates from area a30m as it has large aggregates of layer II neurons (arrows in Fig. 15B, NeuN) and ascending clusters of NFP+ dendrites pass by these islands. Figure 11C shows a thionin-counterstained, SMI32 section of area a30l. Dendritic bundles are marked with arrows and islands of layer II neurons with arrowheads and the former pass by many of the latter. Further, some islands are surrounded by SMI32+ dendrites and appear as chalices (arrowheads with asterisks). Finally, the broad layers II–IV are marked by moderate GAD staining and relatively heavy PV expression. Thus, there are many criteria that distinguish area a30m from a30l.

The posterior divisions of area 30 have a thick layer IV, but share some similarities to their anterior counterparts including broad layers II or II–III and a similarity in the thickness of deeper layers (Fig. 15C, D; NeuN). The heavy NFP plexus in layer II–III in area a30m is present in area

p30m, but at a reduced density, while areas a30m and p30m have much reduced NFP plexuses in this layer. The layer IV GAD plexus is particularly noticeable in area p30m, while it is quite broad throughout superficial layers in both divisions of area 30l. Finally, areas a30m and p30m have dense PV+ dendritic plexuses in layers Ia, and II–III, while those in layer Vb of areas a30l and p30l are more dense and include a greater number of labeled somata.

Discussion

The flat map revision of an earlier 9-area map (Vogt et al. 1986) shows new area subdivisions based on immunohistochemistry and the flattening procedure shows more accurately the extent of RSC because area 29a lies over the superior colliculus and the lateral divisions of area 30 are not exposed on the medial surface. A total of 20 cingulate areas are now distinguished. New areas include ACC area 33, and retrosplenial areas 30l and s29a. New subareas include dorsal and ventral divisions of area 32, anterior and posterior divisions of MCC, and anterior and posterior divisions of areas 30m and 29b. Area 29a begins in a subsplenial position caudal to area s29a and extends horizontally over the superior colliculus. The centroid localization strategy used here can be employed by investigators with the same or different histological preparations to map cingulate areas for further quantitative, connection and/or functional studies.

Localization of Fox-3

We have used NeuN for more than a decade to study cytoarchitecture (Vogt et al. 2001), because it labels somata with a greater intensity than Nissl stains and does not co-label glia (Mullen et al. 1992). Kim et al. (2009) subsequently identified the antigen as Fox-3 and reported it to be almost exclusively localized to rat neuronal nuclei and associated with polypyrimidine tract binding protein associated splicing factor (PSF; Kim et al. 2011). While analyzing neuron somal sizes with NeuN for the present study, many apical dendrites, particularly of large pyramids, contained nodules of Fox-3. Closer analysis showed granules of NeuN that are smaller than nodules and striations between granular deposits. Further, in rare cases of ideal section and intensity of perikaral reactions, plasmalemmal associations were also noted. The striations between granular deposits may indicate trafficking between these structures and imply differential RNA editing functions. Thus, the rabbit cortex may have particular value to study further the functions of Fox-3 and its associated RNA splicing proteins as these localizations have not been identified in rodents.
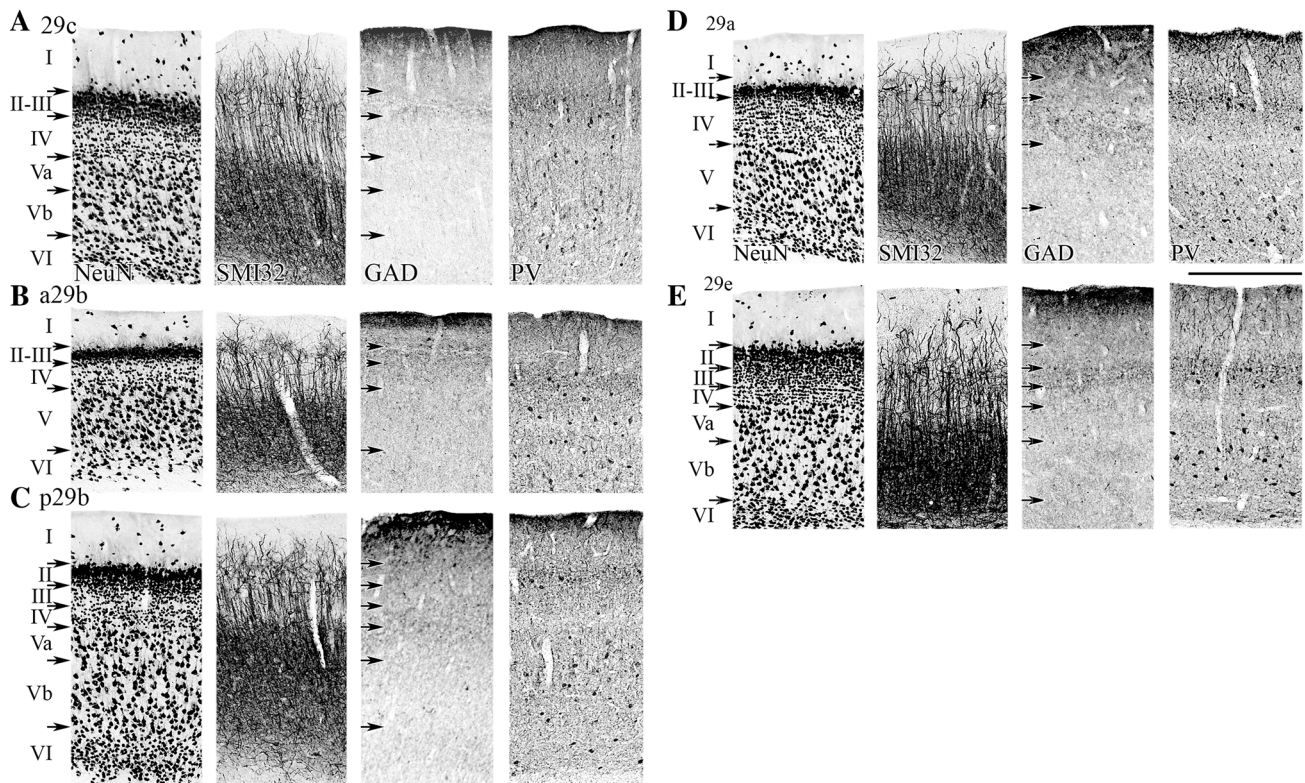
Fig. 14 Details of granular retrosplenial cytology with photographs taken at the *asterisks* in Fig. 12. Differentiation of granular areas from dorsal to ventral positions is apparent particularly in the SMI32 preparations. *Scale bar* 500 μm

Localization of neurofilament proteins

The present study emphasizes the value of NFP expression in identifying cingulate areas in the rabbit; particularly for differentiating the two parts of MCC. The value of this marker, however, extends beyond cytology as these neurons likely have unique projections. Hof et al. (1995) evaluated the proportions of NFP+ neurons that have cortical projections in the monkey. They reported that neurons with long association projections among frontal, parietal, temporal and cingulate cortices were enriched in NFP (45–90 %), whereas short corticocortical connections had much lower numbers of such neurons (4–35 %). Similar observations were made in cingulate motor area projections to primary motor cortex (Nimchinsky et al. 1996). These observations suggest that aMCC may have long corticocortical connections that are less prominent in area p24. Thus, the significance of these neurons lies in their reflection of connectivity patterns and this provides an important new area for further research.

Comparative issues

The conclusions of Brodmann (1909) in rabbits and primates raise a number of comparative issues than can be

addressed with the present observations. His placement of area 23 between anterior and retrosplenial cortices in rabbit was provisional as he recognized that this cortex is agranular and not granular as it is in primates; he had not yet devised the midcingulate concept to resolve this paradox. The observation of a two-part MCC in rabbit is based on NeuN and SMI32 preparations, while the lack of such a distinction in rat was based on Nissl staining (Vogt and Paxinos 2014) and the question remains as to whether or not there is a rabbit-equivalent aMCC in the rat based on similar methods. Figure 16 shows the rabbit area a24a′ NFP expression (see also Fig. 5 for adjacent NeuN) and rostral and caudal parts of rat (hooded, Long-Evans male, 265 gm) MCC area 24a′. Layer Va in rat rostral MCC has few NFP-expressing neurons and there are virtually none in caudal MCC. The rat area 24a′ has a moderate density of NFP+ neurons in layer II both rostrally and caudally, while the rabbit has no such neurons. One difference between the rostral and caudal parts of rat MCC is the presence of more small, NeuN+ neurons throughout the former part; however, this was not recognized as relevant to the distinctions between these areas in rabbit MCC. Also, the caudal part of rat area 24a′ has slightly larger layer III neurons, but this does not rise to the level of a two-part MCC. Thus, based on NFP expression, the rat MCC is not equivalent to either
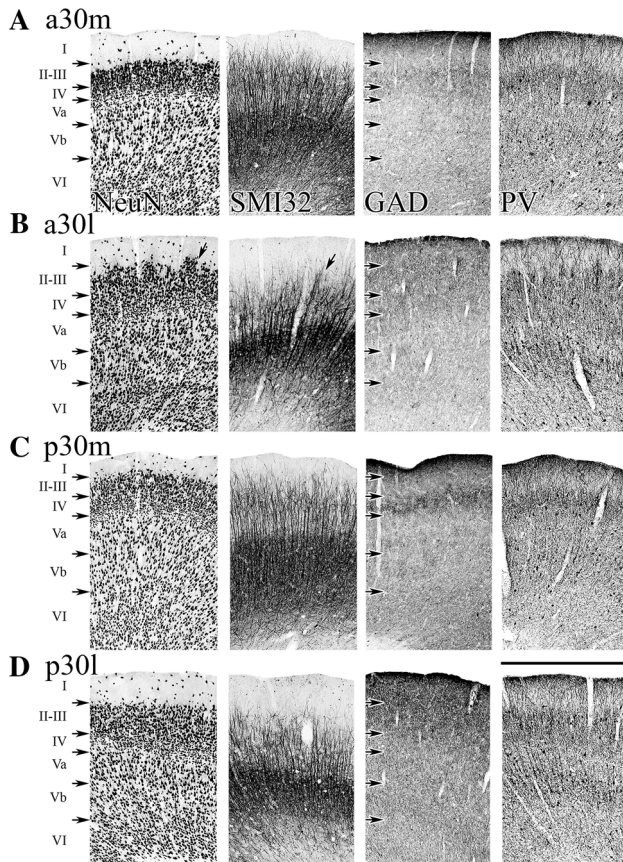
Fig. 15 Cytology of areas a30l/m and p30l/m. The *arrows* for area a30l refer to large islands of layer II neurons (NeuN), clusters of dendrites likely passing by one such island (SMI32), and a PV+ dendritic plexus and somata likely in an island. The area 30 complex is used to designate these areas rather than dysgranular as most of them have a robust layer IV as shown with NeuN. *Scale bar* 500 μm

MCC area in rabbit. Further, the SMI32 immunoreaction is similar in rat rostral and caudal MCC.

As similar Brodmann area designations are often used among species, an area was chosen that meets most of the essential criteria for homology, area a30m, to evaluate the validity of this approach. Figure 17 shows area a30m in rabbit and monkey (male, cynomolgus, 4.3 kg) at the same magnification with pairs of NeuN (A) and SMI32 (B) reacted sections. Layer I in rabbit is 16 % of total cortical depth, while in monkey it is only half of this at 8 %. Layers II and III are very dense and compressed in the rabbit and the latter layer is not differentiated as in monkey. The rabbit has a substantially higher density of NFP-expressing dendrites than monkey and in layer II there are no such processes in monkey like there are in rabbit. In spite of those differences, both species have a dysgranular layer IV (Fig. 17A, R a30m) which is critical to define this area and layer III neurons express high levels of NFP as do those in layers IIIab and IIIc in monkey (Fig. 17B). Thus, while the homology is weak, the relative position of each area in the cingulate cortex justifies a similar designation.

Brodmann (1909) identified an area 26 in the rabbit just ventral to the splenium of the corpus callosum. Area s29a is in this location in the revised map presented in Fig. 2 and it does not appear to be homologous to primate area 26. In the human brain, area 26 is essentially an external granular layer (Braak 1979) with many NFP-expressing neurons (Vogt et al. 2001) and there is virtually no layer V. In contrast, while rabbit area s29a has a dense granular layer II-III, these neurons do not express NFP and only a few neurons in layer V do so. Also, there are large pyramids in layer V (Fig. 13, NeuN) that are not present in human.
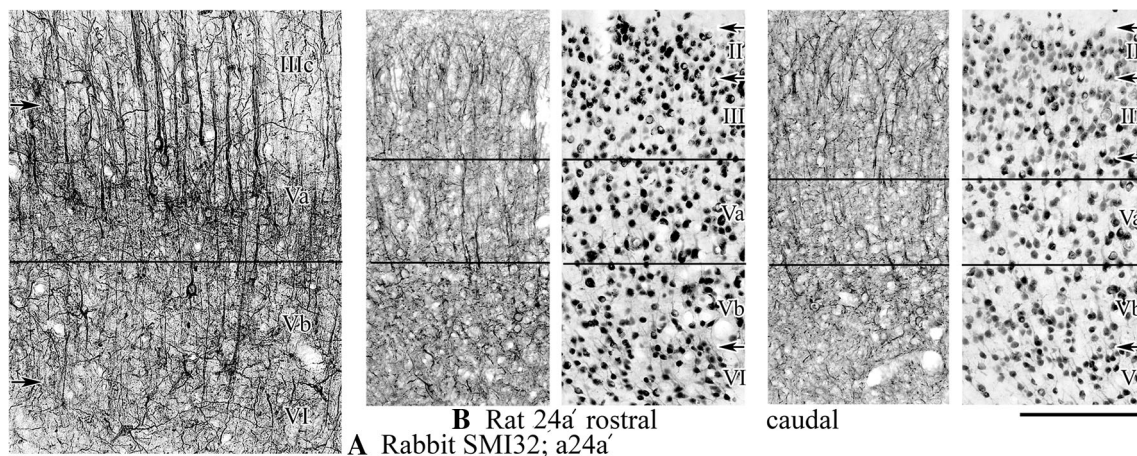

Fig. 16 Comparisons of rabbit SMI32 and rat (pairs of SMI32 and NeuN sections) MCC. Layers aligned at the layer Va/Vb border. **A** Rabbit area a24a′ has a substantially greater number of SMI32-immunoreactive neurons than either the rostral or caudal parts of rat area 24a′. This argues against a dichotomous MCC in rat, although there are a few minor differences in NeuN staining. *Scale bar* 200 μm
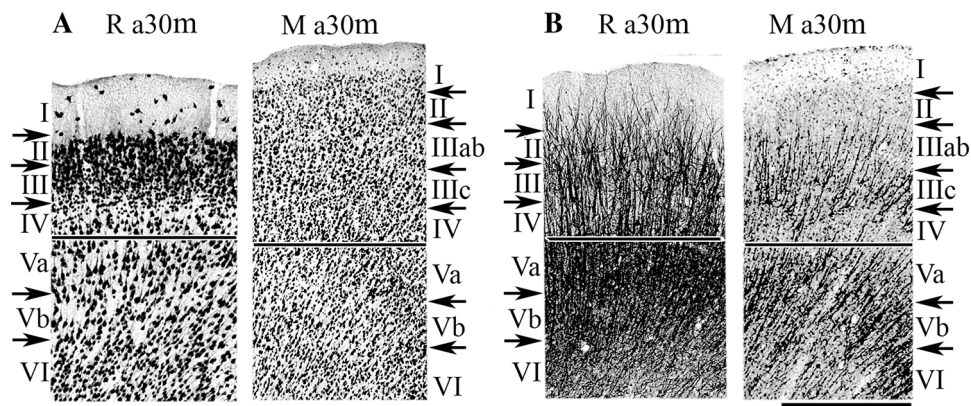
Fig. 17 Photographs of pairs of rabbit (R) and monkey (M) area 30m (**A** NeuN; **B** SMI32). All *photographs* were taken at the same magnification and suggest that rabbit neurons (NeuN) are generally larger than those in monkey. Sections were aligned at the layer IV/Va border to enhance comparisons. While there are many differences between these species the designation is useful in terms of layer IV and the position of area a30m in relationship to other areas. *Scale bar* 500 μm

Fig. 18 Comparison of rabbit and rat flat maps at the same magnification (*scale bar* 2 mm; rat map from Vogt and Paxinos 2014). Each region is similarly color coded and long *arrows emphasize* borders between the three cingulate regions in each species. *Short arrows* denote subregional borders. The substantial rostral extent of ACC is apparent in rabbit as are the subregions of MCC and extensive expansion of the area 30 complex and areas 29a and 29b in comparison to the rat
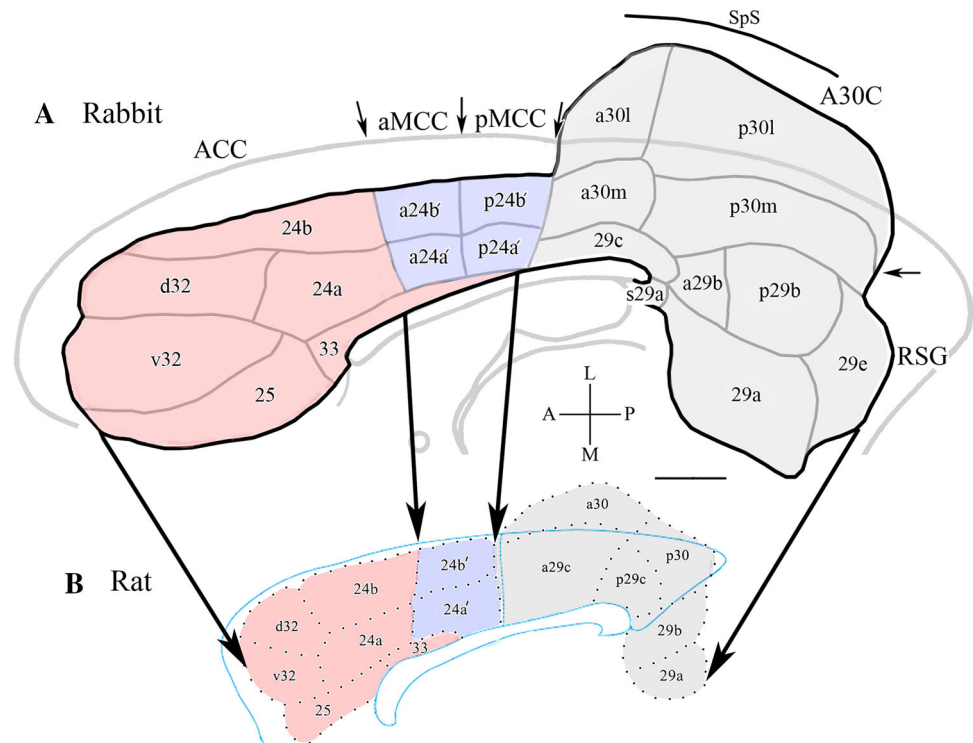
Thus, rabbit area s29a is unique and does not have an equivalent in human.

Overall, the rabbit cingulate cortex is substantially different from the rat as shown in Fig. 18 where the size of each map has been matched. Major differences in the rabbit include rostral expansion of area 32, a two-part MCC, medial and lateral subdivisions of area 30, the latter of which borders visual cortex, a two-part area 29b and an area 29e. The only major differentiation in rat not present in rabbit is the two-part composition of area 29c. Rabbit area 29a is also substantially expanded caudally and this

was not apparent in the earlier map in which flattening was not undertaken (Vogt et al. 1986) because area 29a lies dorsal to the superior colliculus in a horizontal position and it does not appear on the medial surface. Finally, all but one division of area 30 is granular in the rabbit while both divisions of area 30 in rat are dysgranular.

Organization and functions of MCC

The two-part MCC is of critical significance for studies of nociception as noted earlier. The aMCC is particularly

noteworthy with its very large, NFP-expressing layer Va pyramidal neurons. Some of these layer V neurons may project to the pontine nuclei as a major projection that appears to be mainly from MCC in the rat (Wiesendanger and Wiesendanger 1982) and it is possible this is a distinguishing feature of MCC in rabbit. Further, parataenial thalamic projections in rat terminate mainly in areas d32, v32 and 25 with less to 24b and almost none to MCC (Vertes and Hoover 2008; Vogt 2015). This afferent may be a distinguishing feature of ACC and MCC in the rabbit.

A theory of MCC function has been proposed based on intracingulate connections in rat (Vogt 2015) and may be applicable to the rabbit. Both extremes of cingulate cortex, area 32 rostrally and areas 29b/29a caudally, have projections limited to rostral and caudal cingulate cortex, respectively. Buchanan et al. (1994) reported that rabbit ACC intracingulate projections were limited mainly to ACC with minor projections to MCC and none to RSC. In contrast, MCC in rat receives robust projections from both cingulate extremes and projects extensively within the entire cingulate cortex. The ACC and RSC are involved in egocentric (autonomic, somatosensory including internal responses to noxious stimulation and emotional states and memories) and allocentric (visual and auditory cues to navigate through space) functions. The MCC may select the relevant strategy to solve a problem and provide bidirectional feedback about progress toward specific goals and assessment of mismatches with expectations. Vann and Aggleton (2005) placed bilateral lesions in rat area 30 and showed they are capable of employing different strategies to solve the same problem, in this instance the radial-arm maze, by biasing the strategy used to solve the task in the light or dark. Rats with area 30 lesions are less reliant on distal visual cues in the dark to control performance and instead depend on a motor turning strategy to solve the task. Lukoyanov and Lukoyanova (2006) showed that lesions of rat area 30 impaired acquisition of an active avoidance task, while sparing fear-based emotional memory; the latter of which likely depends on ACC and amygdala interactions. As direct interactions between ACC and RSC are weak, MCC may intervene to resolve the behavioral relevance and use of different cues.

Connection studies

Cingulothalamic interactions differ significantly among the various cingulate areas given their substantial differences in layer VI with some areas hardly having a layer VI, while others have a robust layer VI (ACC areas 24a/b and d32, aMCC, posterior divisions of areas 30m, 30l, and 29b). Buchanan et al. (1989) early reported that layers V and VI neurons in rabbit ACC project to the mediodorsal,

ventromedial and paracentral thalamic nuclei and a layer VI projection from RSC to the anterior thalamic nuclei arises from layer VI in rat (Sripanidkulchai and Wyss 1987). Although the functions of cingulothalamic projections are poorly understood, electrical stimulation of rabbit ACC evokes cardiovascular adjustments like those during Pavlovian conditioning and is associated with elevated glucose metabolism in the mediodorsal nucleus (Buchanan et al. 1984). In addition, electrical stimulation of rat ACC enhances nociceptive responses of neurons in the centrolateral thalamic nucleus suggesting a role in feedback pain modulation (Zhang and Zhao 2010).

Shibata and Honda (2012, 2015) described anterodorsal thalamic (AD) and anteroventral (AV) thalamic afferents in rabbit. As is true for the rat (Sripanidkulchai and Wyss 1986), these projections separate into different laminar patterns in each retrosplenial area. Of particular interest, however, is the segregation of AD and AV inputs to anterior and posterior area 30 with the caudal nuclei projecting to area a30 and the rostral nuclei projecting to area p30. In view of the present findings, anterior thalamic afferents to the area 30 complex in rabbit will need reconsideration in the context of numerous cytoarchitectural differentiations. Further, the 20 cingulate areas identified in the present analysis require a comprehensive assessment of thalamic and corticocortical afferents.

Compliance with ethical standards

Conflict of interest The author has no conflict of interest to declare.

References

Ballantine HT, Cassidy WL, Flanagan NB, Marino R Jr (1967) Stereotaxic anterior cingulotomy for neuropsychiatric illness and intractable pain. J Neurosurg 26:488–495

Braak H (1979) Pigment architecture of the human telencephalic cortex IV. Regio retrosplenialis. Cell Tissue Res 204:431–440

Brodmann K (1909) Vergleichende Lokalisationslehre der Grosshirnrinde in ihren Prinzipien dargestellt auf Grund des Zellenbaues. Barth, Leipzig

Buchanan SL, Powell DA, Buggy J (1984) H-2-Deoxyglucose uptake after electrical stimulation of cardiovascular sites in anterior medial cortex in rabbits. Brain Res Bull 13:371–382

Buchanan SL, Powell DA, Thompson RH (1989) Prefrontal projections to the medial nuclei of the dorsal thalamus in the rabbit. Neurosci Lett 106:55–59

Buchanan SL, Thompson RH, Maxwell BL, Powell DA (1994) Efferentconnections of the medial prefrontal cortex in the rabbit. Exp Brain Res 100:469–483

Farrell MJ, Laird AR, Egan GF (2005) Brain activity associated with painfully hot stimuli applied to the upper limb: a meta-analysis. Hum Brain Map 25:129–139

Gabbott PLA, Warner TA, Jays PRL, Salway P, Busby SJ (2005) Prefrontal cortex in the rat: projections to subcortical autonomic, motor, and limbic centers. J Comp Neurol 492:145–177

Hof PR, Nimchinsky EA, Morrison JH (1995) Neurochemical phenotype of corticocortical connections in the macaque monkey—Quantitative analysis of a subset of neurofilament protein immunoreactive projection neurons in frontal, parietal, temporal and cingulate cortices. J Comp Neurol 362:109–133

Kim KK, Adelstein RS, Kawamoto S (2009) Identification of neuronal nuclei (NeuN) as Fox-3, a new member of the fox-1 gene family of splicing factors. J Biol Chem 284:31052–31061

Kim KK, Kim YC, Adelstein RS, Kawamoto S (2011) Fox-3 and PSF interact to activate neural cell-specific alternative splicing. Nucleic Acids Res 39(8):3064–3078. doi:10.1093/nar/gkq1221

Lukoyanov NV, Lukoyanova EA (2006) Retrosplenial cortex lesions impair acquisition of active avoidance while sparing fear-based emotional memory. Behav Brain Res 173:229–236

Mullen RJ, Buck CR, Smith AM (1992) NeuN, a neuronal specific nuclear protein in vertebrates. Development 116:201–211

Nimchinsky EA, Hof PR, Young WG, Morrison JH (1996) Neurochemical, morphologic, and laminar characterization of cortical projection neurons in the cingulate motor areas of the macaque monkey. J Comp Neurol 374:136–160

Porro CA, Baraldi P, Pagnoni G, Serafini M, Facchin P, Maieron M, Nichelli P (2002) Does anticipation of pain affect cortical nociceptive systems? J Neurosci 22:3206–3214

Porro CA, Cettolo V, Francescato MP, Baraldib P (2003) Functional activity mapping of the mesial hemispheric wall during anticipation of pain. Neuroimage 19:1738–1747

Shibata H, Honda Y (2012) Thalamocortical projections of the anterodorsal thalamic nucleus in the rabbit. J Comp Neurol 520:2647–2656

Shibata H, Honda Y (2015) Thalamocortical projections of the anteroventral thalamic nucleus in the rabbit. J Comp Neurol 523(5):726–741

Sripanidkulchai K, Wyss JM (1986) Thalamic projections to the retrosplenial cortex in the rat. J Comp Neurol 254:143–165

Sripanidkulchai K, Wyss JM (1987) The laminar organization of efferent neuronal cell bodies in the retrosplenial granular cortex. Brain Res 406:255–269

Talairach J, Bancaud J, Geier S, Bordas-Ferrer M, Bonis A, Szikla G (1973) The cingulate gyrus and human behavior. Electroencephalogr Clin Neurophysiol 34:45–52

Vann SD, Aggleton JP (2005) Selective dysgranular retrosplenial cortex lesions in rats disrupt allocentric performance of the radial-arm maze task. Behav Neurosci 119:1682–1686

Vertes RP, Hoover WB (2008) Projections of the paraventricular and paratenial nuclei of the dorsal midline thalamus in the rat. J Comp Neurol 508:212–237

Vogt BA (1993) Structural organization of cingulate cortex: areas, neurons, and somatodendritic transmitter receptors. In: Vogt BA, Gabriel M (eds) Neurobiology of cingulate cortex and limbic thalamus. Birkhauser, Boston, pp 19–70

Vogt BA (2005) Pain and emotion interactions in subregions of the cingulate gyrus. Nat Rev Neurosci 6:533–544

Vogt BA (2015) Cingulate cortex and pain architecture. In: Paxinos G (ed) The rat nervous system, vol 4. Elsevier, Amsterdam

Vogt BA, Paxinos G (2014) Cytoarchitecture of mouse and rat cingulate cortex with human homologies. Brain Struct Funct 219:185–192

Vogt BA, Sikes RW (2009) Cingulate nociceptive circuitry and roles in pain processing: the Cingulate Premotor Pain Model. In: Vogt BA (ed) Cingulate neurobiology and disease. Oxford University Press, London

Vogt BA, Sikes RW, Swadlow HA, Weyand TG (1986) Rabbit cingulate cortex: cytoarchitecture, physiological border with visual cortex and afferent cortical connections including those of visual, motor, postsubicular and transcingulate origin. J Comp Neurol 248:74–94

Vogt BA, Nimchinsky EA, Vogt LJ, Hof PR (1995) Human cingulate cortex: Surface features, flat maps, and cytoarchitecture. J Comp Neurol 359(3):490–506

Vogt BA, Vogt LJ, Perl DP, Hof PR (2001) Cytology of human caudomedial cingulate, retrosplenial, and caudal parahippocampal cortices. J Comp Neurol 438:353–376

Vogt BA, Vogt LJ, Farber NB, Bush G (2005) Architecture and neurocytology of monkey cingulate gyrus. J Comp Neurol 485(3):218–239

Vogt BA, Mohlberg H, Zilles K, Amunts K, Palomero-Gallagher N (2016) Human retrosplenial cortex: cytoarchitecture and probability maps. In preparation

Wiesendanger R, Wiesendanger M (1982) The corticopontine system in the rat: I. Mapping of corticopontine neurons. J Comp Neurol 208:215–226

Zhang L, Zhao Z-Q (2010) Plasticity changes of neuronal activities in central lateral nucleus by stimulation of the anterior cingulate cortex in rat. Brain Res Bull 81:574–578